

# BEAM: Bridging Physically-based Rendering and Gaussian Modeling for Relightable Volumetric Video

Yu Hong<sup>1,2\*</sup> Yize Wu<sup>1\*</sup> Zehao Shen<sup>1,2</sup> Chengcheng Guo<sup>1,2</sup> Yuheng Jiang<sup>1†</sup>  
 Yingliang Zhang<sup>3</sup> Jingyi Yu<sup>1</sup> Lan Xu<sup>1</sup>  
<sup>1</sup>ShanghaiTech University <sup>2</sup>NeuDim <sup>3</sup>DGene



Figure 1. We present BEAM, a novel pipeline that bridges 4D Gaussians with accurate physically-based rendering to produce relightable volumetric videos, delivering immersive and realistic experiences on platforms such as VR.

## Abstract

Volumetric video enables immersive experiences by capturing dynamic 3D scenes, enabling diverse applications for virtual reality, education, and telepresence. However, traditional methods struggle with fixed lighting conditions, while neural approaches face trade-offs in efficiency, quality, or adaptability for relightable scenarios. To address these limitations, we present BEAM, a novel pipeline that bridges 4D Gaussian representations with physically-based rendering (PBR) to produce high-quality, relightable volumetric videos from multi-view RGB footage. BEAM recovers detailed geometry and PBR properties via a series of available Gaussian-based techniques. It first combines Gaussian-based performance tracking with geometry-aware rasterization in a coarse-to-fine optimization framework to recover spatially and temporally consistent geometries. We further enhance Gaussian attributes by incorporating PBR properties step by step. We

generate roughness via a multi-view-conditioned diffusion model, and then derive AO and base color using a 2D-to-3D strategy, incorporating a tailored Gaussian-based ray tracer for efficient visibility computation. Once recovered, these dynamic, relightable assets integrate seamlessly into traditional CG pipelines, supporting real-time rendering with deferred shading and offline rendering with ray tracing. By offering realistic, lifelike visualizations under diverse lighting conditions, BEAM opens new possibilities for interactive entertainment, storytelling, and creative visualization.

## 1. Introduction

Volumetric video captures dynamic 3D scenes from multiple angles, allowing interactive viewing from any perspective. This technology is crucial for creating immersive experiences in virtual and augmented reality, enhancing storytelling, education, cultural preservation, and telepresence with lifelike, interactive content. However, traditional vol-

\* Equal contribution. † Project Leader.

umetric video is often limited by fixed lighting conditions captured during recording, which can clash with dynamic or virtual environments, reducing realism and flexibility. Relightable volumetric video overcomes this limitation by enabling post-capture relighting. This allows for seamless integration into dynamic lighting environments and offers creative control over visual aesthetics.

The prevailing workflow [7, 14, 19, 36] for producing relightable volumetric videos in the industry still relies on tracked mesh sequences and texture videos, which can be seamlessly integrated into standard CG pipelines to support relighting under various lighting conditions. However, the intricate reconstruction process often introduces artifacts such as holes and noise, and the quality of relighting remains constrained, frequently resulting in visible imperfections. Neural advancements [56, 74, 81] focus on enabling relighting capabilities using neural factorization within implicit MLPs representations. However, these approaches often face challenges in balancing training efficiency, rendering speed, and output quality, ultimately failing to deliver satisfactory results. Recently, 3D Gaussian Splatting (3DGS)[35], an efficient point-based representation, has achieved photo-realistic rendering at unprecedented frame rates. While dynamic variants[30, 38, 65] can produce high-quality volumetric videos, they fail to produce the detailed geometry necessary for essential operations like relighting. Although efforts [18, 32, 40, 54] have been made to integrate physically-based rendering into the 3DGS pipeline, these methods are often computationally expensive and limited to static scenarios. These limitations severely restrict their applicability in industrial workflows, hindering the efficient production of 4D content.

In this paper, we introduce BEAM, a novel pipeline that bridges 4D Gaussians with accurate physically-based rendering (PBR) for producing relightable volumetric videos from multi-view RGB footage. Our key idea is to robustly recover detailed geometry and decouple the PBR properties (e.g., ambient occlusion, roughness, and base color) using a carefully selected suite of techniques, i.e., rasterization, performance tracking, and ray tracing, all within a Gaussian-based paradigm. As a result, BEAM enables lifelike dynamic scenes that can be seamlessly and CG-friendly integrated into various platforms under diverse lightings (see Fig. 1).

We first recover detailed and spatial-temporally consistent geometries from multiview video input, which organically combines the Gaussian-based performance tracking [30] with the geometry-aware Gaussian rasterization [78]. While the former excels at motion tracking and the latter at static geometry recovery, we unify them in a coarse-to-fine optimization framework. Specifically, we employ coarse joint Gaussians to track non-rigid motion and dense skin Gaussians to preserve intricate geometry

details. We adopt a robust optimization process that integrates normal consistency, photometric consistency, and temporal regularization to enhance geometric accuracy and smoothness. This enables accurate depth and normal recovery from the dense Gaussians using the geometry-aware rasterizer [78], providing a robust foundation for material decomposition and relighting.

We further decouple the dense 4D Gaussians to recover detailed material properties, enabling high-quality physically-based rendering grounded in the rendering equation [33] and simplified Disney BRDF [2]. Assuming human-centric scenes with negligible metallic components, we focus on accurately associating roughness, ambient occlusion (AO), and base color properties with the Gaussians, ensuring realistic and adaptable rendering under diverse lighting conditions. To achieve this, we adopt a step-by-step approach to disentangle these properties. Specifically, we first generate a roughness texture using the material diffusion module in previous work [79] with multi-view conditioning, which is associated with the dense Gaussians through UV projection. Then, for the AO and base color, we adopt a 2D-to-3D strategy, where these attributes are estimated in the input views to bake 2D material maps, and then optimize into the corresponding dense Gaussians in the 3D space. This strategy effectively reduces noise and smooths the disentanglement to improve relighting quality. For further 2D AO and based color decomposition, the lighting environment during capturing can be estimated using off-the-shelf tool [47], while the geometry attributes and roughness are obtained in previous stages. Thus, by carefully re-examining and simplifying the rendering equation [33], we identify a critical insight: both 2D AO and base color can be accurately derived by accumulated visibility information for specific points along specific directions during ray tracing. We tailor the Gaussian-based ray tracer [45] to compute such visibility, with a novel alpha blending strategy based on the dense Gaussians. This strategy efficiently captures visibility information, forming the foundation for estimating AO and base color maps in the input viewpoints.

Once the material properties are baked into our dense dynamic Gaussians, these 4D assets seamlessly integrate with traditional CG engines, supporting flexible rendering workflows. For real-time rendering, we adopt deferred shading to deliver immersive and efficient visualizations, while offline rendering leverages ray tracing to precisely capture complex shadows and occlusions. We further develop a Unity plugin enabling seamless integration of 4D assets into various platforms for real-time, lifelike interactions under diverse lighting conditions. This innovation opens new possibilities for storytelling, interactive entertainment, and creative visualization, offering users an immersive journey into dynamic, relightable volumetric worlds.

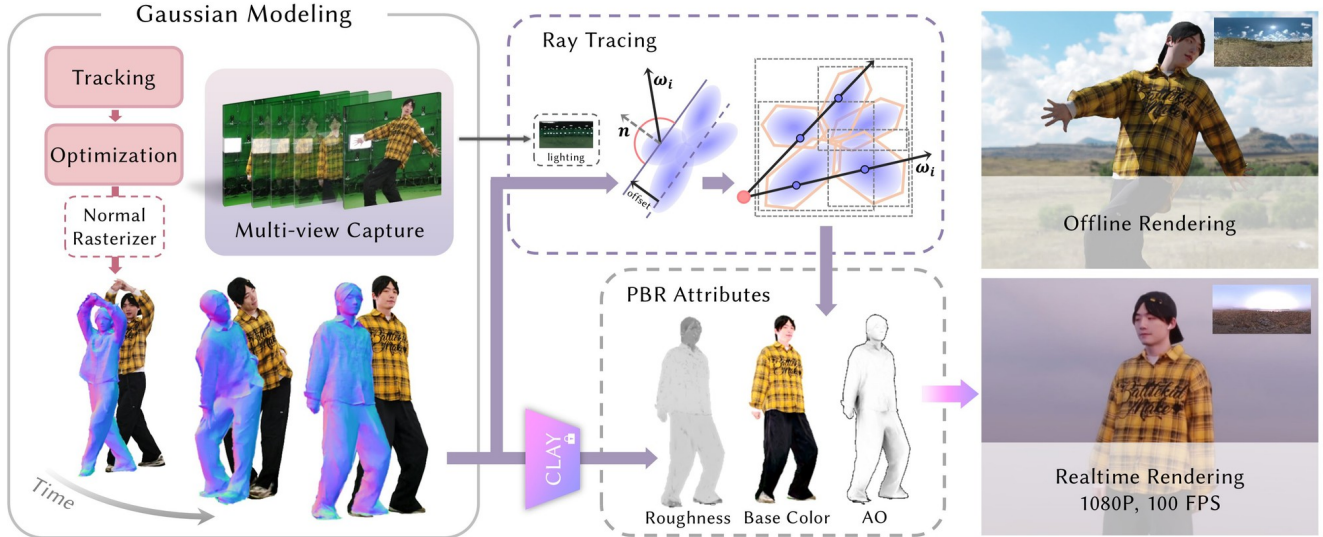


Figure 2. We propose a novel BEAM method to produce Gaussian sequences. We first use tracking results of joint Gaussians and a normal regularizer to obtain our 4D Gaussians with consistent geometry. Then we infer roughness using a generative model and apply ray tracing to compute the 2D base color and AO maps, which are then used to optimize the corresponding Gaussian attributes. Our results can be rendered under varying lighting conditions using both real-time and offline rendering.

## 2. Related Work

**Human Modeling** In the field of Human Modeling, numerous methods [17, 57, 60, 82] have been proposed to address these challenges. Li [37] integrates temporal denoising into non-rigid mesh template tracking to capture detailed geometry, while High-quality FVV [7] compactly represents human performance using tracked mesh sequences and textured video.

With the advancement of neural rendering techniques [44], several works have incorporated time as a latent variable to handle dynamic scenes [50, 62, 70]. Meanwhile, other approaches [22, 48, 49, 58, 66, 84, 85] leverage the human parametric model [41] to reconstruct the animatable avatar. Furthermore, some hybrid methods [27, 28, 75] combine explicit volumetric fusion with implicit neural techniques to capture more details. Additionally, several methods [26, 28, 53, 55, 64] significantly accelerate training and rendering speed, by leveraging advanced data structures such as voxel grids [16], hash tables [46], and tensor decomposition [4]. Recently, 3DGS [35] ensures both high quality and fast rendering, while dynamic variants [15, 24, 31, 38, 42, 59, 69, 72, 73] enable complex 4D scene reconstruction for advanced human modeling. DualGS [30] uses joint and skin Gaussians to capture motion and detailed appearance. However, these approaches fail to recover detailed geometry and do not support relighting.

**Human Relighting** Human Relighting aims to manipulate the reflectance field of the human surface, enabling an immersive fusion with novel illumination. Conven-

tional methods [3, 9–11, 21, 23, 67, 68] use LightStage systems to capture human reflectance characteristics, requiring costly controlled lighting and dense camera arrays that are not widely accessible. In 2D image-based relighting tasks, previous methods [34, 61] rely on convolutional networks for inference, while recent diffusion-based approaches [13, 77] leverage generative models to learn complex light interactions across large datasets. However, the lack of a 3D representation makes it challenging to maintain 3D consistency of lighting. In addition, some neural relighting methods [1, 76, 81] use NeRF [44] for 3D reconstruction of material properties and lighting effects. However, their rendering quality is inadequate and hard to integrate with traditional CG pipelines. Recent methods [18, 20, 32, 40] leverage 3DGS representation for relighting due to its ability to reconstruct fine details and interaction in CG engines. For human performance relighting, researchers [5, 6, 39, 43, 71, 83] extend mesh-based and neural relighting methods by incorporating body pose priors [29, 41]. However, avatars relying on skeletal priors struggle with complex clothing, wrinkles, and human-object interactions.

## 3. Method

Given multi-view video inputs, we aim to produce relightable 4D Gaussian sequences with physically-based rendering (PBR) materials, enabling realistic rendering under various lighting. PBR typically requires multiple material components, such as base color, metallic, roughness, normal, and ambient occlusion (AO), as shown in Fig.3. In our



approach, as the metallic attribute is negligible for human bodies, we set it to zero and focus on optimizing the remaining properties: normal, roughness, AO, and base color. The complete pipeline is illustrated in Fig.2.

### 3.1. Gaussian Modeling and Geometry Optimization

To obtain temporally consistent geometric information (depth and normal maps) for physical-based rendering, we seamlessly combine the Gaussian-based performance tracking [30] with the geometry-aware rasterizer [78] within a coarse-to-fine optimization framework. Specifically, our framework uses a dual Gaussian representation to separately model global motion and visual appearance through joint and skin Gaussians. Each skin Gaussian is anchored to multiple joint Gaussians and is warped across frames based on the tracking results of these joint Gaussians. The optimization process integrates a photometric loss  $E_{\text{color}}$ , a rigid term  $E_{\text{rigid}}$ , and a temporal regularization term  $E_{\text{temp}}$ .

To further enhance the optimization of Gaussian geometry, we introduce an additional normal consistency loss  $E_{\text{normal}}$ . During rasterization, we assume that the intersection points between rays and Gaussians correspond to the maxima in Gaussian values. The depth of a Gaussian is defined as the depth of the intersection point, while the normal of the intersection plane is taken as the Gaussian normal. This rasterizing process generates precise depth maps and normal maps  $N_r$ . Using the obtained depth map, we compute the normal map  $N_d$  based on a local plane assumption and then measure the normal consistency loss  $E_{\text{normal}}$  between  $N_d$  and  $N_r$  as follows:

$$E_{\text{normal}} = \sum_i \omega_i (1 - N_r^T N_d), \quad (1)$$

where  $i$  indexes the intersected splats along the ray, and  $\omega_i = \alpha_i \prod_{j=1}^{i-1} (1 - \alpha_j)$  represents the blending weight of the intersection point.

The total energy term in our 4D Gaussian modeling and geometric optimization framework is expressed as:

$$E = \lambda_{\text{color}} E_{\text{color}} + \lambda_{\text{smooth}} E_{\text{smooth}} + \lambda_{\text{temp}} E_{\text{temp}} + \lambda_{\text{normal}} E_{\text{normal}}, \quad (2)$$

During dynamic training,  $E_{\text{norm}}$  is introduced after the appearance optimization over 7,000 iterations, followed by an additional 5,000 iterations dedicated to optimizing the normals. For other energy terms not discussed here, please refer to DualGS [30]. The hyperparameters are set as follows:  $\lambda_{\text{color}} = 1$ ,  $\lambda_{\text{smooth}} = 0.001$ ,  $\lambda_{\text{temp}} = 0.00005$ ,  $\lambda_{\text{normal}} = 0.03$ .

### 3.2. PBR Materials Decomposition

To enable physical-based rendering within the Gaussian-based paradigm, we extend 3D Gaussian attributes by incorporating a roughness value and two additional third-order



Figure 3. Illustration of Gaussian properties. We showcase the normal, roughness, AO and base color maps required for relighting, which are rasterized from our relightable 4D Gaussians.



Figure 4. We present the results of different rendering techniques. Real-time rendering focuses on efficiency, while offline rendering delivers more realistic shadows and occlusion effects.

spherical harmonic (SH) properties for AO and base color. And we utilize a step-by-step approach to disentangle these properties.

**Roughness.** To efficiently assign a roughness value to each Gaussian, we utilize a generative model that offers significantly faster performance compared to inverse rendering methods. Specifically, we feed the canonical mesh and multi-view images into the Material Diffusion module of CLAY [79] to generate a roughness texture for the mesh. Each valid pixel of the texture is then mapped back to the world coordinate system, allowing us to assign each Gaussian the roughness value of its nearest pixel.

**Ambient Occlusion and Base Color** For AO and base color, we first estimate these two attributes in the input views for each frame to bake 2D material maps, and then optimize into the corresponding dense skin Gaussians.

Ambient Occlusion  $\mathcal{A}(x)$  is an approximation of global illumination, which models the diffuse shadows produced by close, potentially small occluders within a constrained computational budget:

$$\mathcal{A}(x) = \frac{1}{\pi} \int_{\Omega} V^{\text{env}}(x, \omega_i) (\mathbf{n} \cdot \omega_i) d\omega_i, \quad (3)$$



Figure 5. Gallery of our results. We present some real-time rendering results under HDRI settings, which deliver high-fidelity rendering of human performances across challenging motions and complex clothing textures.

where  $V^{\text{env}}(x, \omega_i)$  is the visibility term at 3D point  $x$  in direction  $\omega_i$ ,  $\mathbf{n}$  is the normal of the surface at point  $x$ ,  $\Omega$  is the hemisphere centered in  $x$  and having  $\mathbf{n}$  as its axis.

For the base color, we use a simplified Disney BRDF model [2] composed of a Lambertian diffuse term and a Cook-Torrance specular term [8], with the outgoing radiance  $L_o$  being a linear combination of these two components. Since for dielectric materials the diffuse part is proportional to the base color while the specular part is independent of it, the rendering equation [33] can be written as:

$$L_o(x, \omega_o) = \rho(x)L_o^D(x, \omega_o) + L_o^S(x, \omega_o), \quad (4)$$

where  $L_o(x, \omega_o)$  is the outgoing radiance at  $x$  in direction  $\omega_o$ , computed by mapping image pixel colors to linear space.  $\rho$  is the base color,  $L_o^D$  is the diffuse part residue and  $L_o^S$  is the specular part. To simplify the rendering equation, our computation of the base color disregards the indirect illumination effects caused by surface reflections on the human body. Consequently,  $L_o^D$  and  $L_o^S$  are expressed as follows:

$$L_o^D(x, \omega_o) = \frac{1}{\pi} \int_{\Omega} (1 - F) \mathcal{L}(x, \omega_i) d\omega_i, \quad (5)$$

$$L_o^S(x, \omega_o) = \int_{\Omega} f_{rs}(x, \omega_i, \omega_o) \mathcal{L}(x, \omega_i) d\omega_i, \quad (6)$$

where  $\mathcal{L}(x, \omega_i) = V^{\text{env}}(x, \omega_i) L_i^{\text{env}}(\omega_i) (\mathbf{n} \cdot \omega_i)$ ,  $F$  is the approximated Fresnel term,  $f_{rs}$  is the specular term in the BRDF,  $L_i^{\text{env}}$  can be queried from the environment map. To capture the environment map of our multi-view, well-lit dome setup, we position a DSLR camera at the center and take bracketed exposure photographs from multiple directions. These photographs are then processed using PTGui [47] to generate a high dynamic range (HDR) panoramic image, enabling precise calculation of the incoming radiance  $L_i^{\text{env}}$  from the environment.

We observe that both 2D AO and base color need the visibility term  $V^{\text{env}}$ . To accurately compute  $V^{\text{env}}$ , we adopt Gaussian ray tracer from 3DGRT [45], and compute intersections based on the maximum Gaussian response. For efficient computation, a proxy icosahedron mesh is employed to leverage hardware acceleration, with a two-level BVH constructed at both the mesh and instance levels. We accumulate the alpha values of the Gaussians at the intersection points without sorting them:

$$\alpha = \sum_{i=1}^N O_i G_i(x_i), \quad (7)$$

where  $O_i$  is the opacity of the  $i_{\text{th}}$  Gaussian,  $G_i(x_i)$  is the response of the Gaussian kernel at  $x_i$  which makes the response be the maximum value along the ray. We set



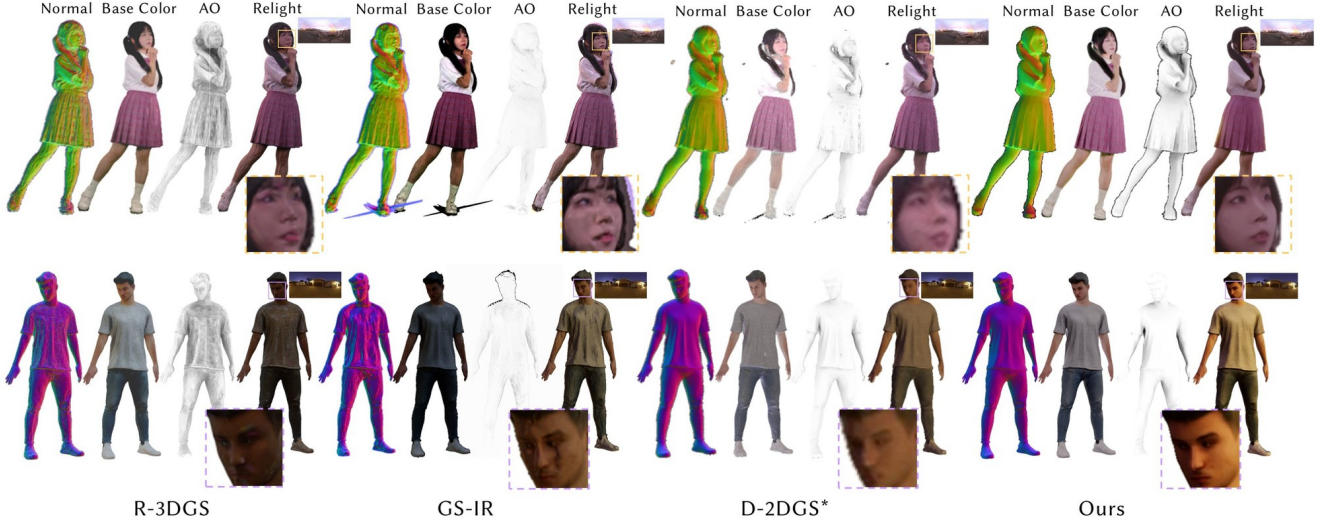


Figure 6. Qualitative comparisons of our method against R-3DGS [18], GS-IR [40] and D-2DGS\* [80]. D-2DGS\* refers to the results of inverse rendering applied to mesh sequences obtained from D-2DGS to decouple PBR materials. Our method achieves the highest relighting quality. For more detailed comparison results, please refer to the appendix.

$V^{\text{env}}(x, \omega_i) = 0$  only when  $\alpha$  is greater than a threshold  $T$  (we choose  $T$  as 0.9999); otherwise,  $V^{\text{env}}(x, \omega_i) = 1$ . Ray tracing stops once the accumulated alpha value exceeds the threshold  $T$ . To avoid occlusion from Gaussians directly above the original depth, we offset the ray origin  $o$  along the normal direction:  $o = x + \epsilon \mathbf{n}$ .

Finally, we use the Monte Carlo method to solve the integrals in Eq. 3, 5, 6. We render the AO image with 50 samples per pixel and the base color image with 100 samples per pixel, then apply Intel Open Image Denoise [25] for denoising.

To optimize the AO and base color material maps into the corresponding dense skin Gaussians, we employ the generated training view material maps as ground truth supervision, while keeping all other geometry-related attributes fixed. The optimization process commences by initializing the AO attributes with zeros and the base color attributes with RGB values. We then train 5000 iterations to obtain both AO and base color attributes separately. Besides, we incorporate the same regularization term to the base color to ensure temporal consistency.

### 3.3. Physically Based Rendering

By leveraging our relightable 4D Gaussians, we can seamlessly integrate the 4D assets into traditional CG engines, supporting both real-time and offline rendering workflows. For real-time rendering, we utilize the deferred shading to deliver immersive and efficient visualization across diverse settings. For offline rendering, we employ ray tracing, which excels in handling shadows and occlusion relationships, ensuring high-quality results.

**Real-time Rendering.** We implement real-time rendering using deferred shading techniques [12], based on the High Definition Render Pipeline (HDRP) in Unity. Specifically, we rasterize our 4D Gaussian sequence with extra PBR attributes, including base color, AO, normals, roughness, and depth maps, and store them in the GBuffer. This GBuffer is then integrated into the original forward transparent stage of HDRP for rendering semi-transparent objects. We also leverage shadow mapping from the HDRP rendering pipeline to perform shadow calculations for Gaussians under different light types. Our approach enables real-time rendering at 100 FPS in 1080P for volumetric videos.

**Offline Rendering.** For offline rendering, we sort the intersection points of the Gaussian during ray tracing, and use alpha blending to determine the exact intersection with the entire Gaussian object, simultaneously acquiring the normal and material attributes at that point. This allows full compatibility with the widely used path tracing pipeline. To demonstrate the relighting quality of real-time rendering and offline rendering techniques, we showcase results for both under an environment map, as depicted in Fig. 4. Notably, the offline rendering effectively handles the shadows caused by occlusions in the Gaussian representations.

## 4. Experiments

To demonstrate our relighting capabilities, we capture human performances with rich textures and challenge body movements using 81 calibrated industrial cameras, enabling high-quality rendering under diverse lighting conditions. Our pipeline is implemented based on 3DGS [35] and

Table 1. Quantitative comparison with SOTA relighting methods on our blender-rendered synthetic dataset. Green and yellow cell colors indicate the best and the second-best results.

Method	AO			Base Color			Relighting		
	PSNR $\uparrow$	SSIM $\uparrow$	LPIPS $\downarrow$	PSNR $\uparrow$	SSIM $\uparrow$	LPIPS $\downarrow$	PSNR $\uparrow$	SSIM $\uparrow$	LPIPS $\downarrow$
R-3DGS	20.67	0.791	0.307	20.65	0.853	0.166	24.66	0.855	0.105
GS-IR	18.95	0.850	0.345	13.35	0.702	0.252	23.05	0.858	0.177
D-2DGS*	24.19	0.906	0.232	21.04	0.839	0.145	23.23	0.857	0.198
Ours	25.32	0.924	0.168	21.47	0.906	0.084	25.57	0.895	0.086

trained on a single NVIDIA GeForce RTX 3090. Our method achieves a processing time of 12 minutes per frame for 4D Gaussians modeling and optimization and 4 minutes for materials estimation and baking. The generated relightable 4D Gaussian sequences are fully compatible with VR platforms and CG engines, enhancing immersive experiences during playback and editing.

### 4.1. Comparison

We compare our method against state-of-the-art static Gaussian relighting techniques, R-3DGS [18], GS-IR [40], both of which reconstruct geometry frame by frame. For dynamic comparison, we first obtain the mesh sequences using D-2DGS [80] and then apply the path replay backpropagation method [63] for inverse rendering to decouple attributes, such as base color and roughness for each frame individually. As shown in Fig. 6, the normals and AO decoupled by Relightable-3DGS are blurry, resulting in significant relighting artifacts. GS-IR struggles to reconstruct smooth normals and effectively separate the base color from other attributes. While D-2DGS with inverse rendering produces smoother normals and more accurate attribute decoupling, the relighting results are prone to losing high-frequency details. In contrast, our method produces smooth normals and accurately decouples the AO and base color, enabling high-fidelity relighting results.

For quantitative comparison, we conduct evaluations on synthetic data to generate ground truth images under predefined lighting conditions. We use Blender to simulate the similar capture perspectives of our dome system and render human meshes from RenderPeople[51] into corresponding viewpoints using the CYCLES engine. We employ PSNR, SSIM, and LPIPS as metrics. To ensure a fair and precise comparison, we compute the metrics for AO, base color, and relighting results across two synthetic sequences, each consisting of 150 frames. In addition, we compute these metrics within the bounding box of the human region. As shown in Tab. 1, our method surpasses the other techniques in all metrics evaluated.

### 4.2. Evaluation

**Materials Decomposition.** We conduct a qualitative ablation study on materials decomposition to the impact of different variables on AO, base color, and the final relighting

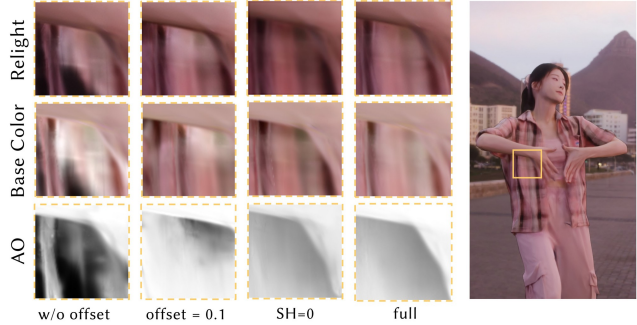


Figure 7. Ablation on parameter settings for materials decomposition. Our full model provides accurate AO and base color representations, resulting in high-quality relighting with minimal artifacts.

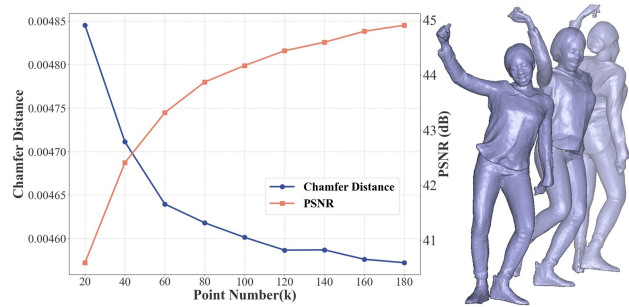


Figure 8. Ablation study on the number of geometry-aware Gaussians. With  $\sim 140,000$  Gaussians, BEAM achieves high rendering quality and geometric reconstruction accuracy, while ensuring efficient training and rendering.

ing results. For the offset variable in the Gaussians surface estimation during ray tracing, we present the results without the offset and with an excessively large offset (0.1), in the first and second columns of Fig. 7. We found that without an offset, AO and base color contained many black artifacts, and the Gaussian surface estimation suffered significant degradation. On the other hand, an offset of 0.1 led to overestimation, causing incorrect lighting decoupling and producing overly bright artifacts. Additionally, regarding the SH order required to represent AO and base color, as illustrated in the third column of Fig. 7, using a zero-order SH Gaussian resulted in blurriness. In contrast, our full ray tracing and material optimization pipeline, with an offset set to 0.02 and using third-order SH degree with geometry-aware Gaussians, provides accurate calculations and representations of the Gaussian’s AO and base color attributes.

**The Number of Gaussians.** We evaluate the impact of varying the number of geometry-aware Gaussians on both rendering quality and mesh quality across 100 frames in our virtual dataset, using PSNR and Chamfer Distance respec-

tively. As shown in Fig. 8, using  $\sim 140,000$  geometry-aware Gaussians strikes an optimal balance between rendering quality and geometric reconstruction accuracy, without introducing excessive redundancy. This point count ensures efficient training and is well-suited for applications such as VR and AR.

### 4.3. User Study

We conduct a user study to evaluate the temporal reconstruction quality and normal consistency of our 4D Gaussians. We assess our method on our captured dataset, comparing it against R-3DGS, GS-IR, as well as D-2DGS, and ask 30 users to select the best option. For GS-IR and R-3DGS, we train Gaussian models for 200 frames individually and concatenate the per-frame normal maps. For our method and D-2DGS, we rasterize a normal map sequence from a 200-frame dynamic Gaussian sequence. In terms of temporal reconstruction quality, 95.65% of users prefer our method, while 87% choose our approach for normal consistency. These preference results clearly indicate a significant advantage of our method over the competing approaches, demonstrating its superior performance in both aspects.

## 5. Conclusion

**Limitations.** Although our method achieves high-quality immersive rendering, there are some limitations. First, the integration of new attributes into the original Gaussian expression will lead to substantial storage requirements for dynamic Gaussian sequences. Future work will consider compressing these sequences. Second, we approximate the rendering equation to obtain the 2D material maps, which introduces errors in our decoupled material results and does not accurately reflect the real physical world. Future work may address this issue by incorporating large models like video generation. Furthermore, our approach, focusing on relighting for a dynamic reconstruction sequence, does not support pose-driven animation or the generation of new poses. Future work will focus on optimizing these aspects to improve robustness and applicability.

We have presented a Gaussian-based approach for reconstructing detailed geometry and PBR materials to produce relightable volumetric videos. We employ a coarse-to-fine training strategy and effective geometric constraints to accurately model the dynamic geometry of 4D Gaussians. Additionally, we decouple PBR materials by using ray tracing to compute the lighting effects and obtain base color and AO maps, while leveraging generative methods to infer roughness. These materials are then baked into the corresponding attributes of the Gaussians. With deferred shading and ray tracing techniques, our Gaussian sequence supports both efficient real-time rendering and more realistic offline rendering. Experimental results demonstrate the advantages of our approach in generating high-quality dynamic normal maps

and material decomposition, as well as its relightability under a variety of lighting conditions. Our method is highly compatible with traditional CG engines, offering significant potential for enhancing rendering realism and flexibility.

## References

- [1] Mark Boss, Raphael Braun, Varun Jampani, Jonathan T Barron, Ce Liu, and Hendrik Lensch. Nerd: Neural reflectance decomposition from image collections. In *Proceedings of the IEEE/CVF International Conference on Computer Vision*, pages 12684–12694, 2021. 3
- [2] Brent Burley and Walt Disney Animation Studios. Physically-based shading at disney. In *Acm Siggraph*, pages 1–7. vol. 2012, 2012. 2, 5
- [3] Charles-Félix Chabert, Per Einarsson, Andrew Jones, Bruce Lamond, Wan-Chun Ma, Sebastian Sylwan, Tim Hawkins, and Paul Debevec. Relighting human locomotion with flowed reflectance fields. In *ACM SIGGRAPH 2006 Sketches*, pages 76–es. 2006. 3
- [4] Anpei Chen, Zexiang Xu, Andreas Geiger, Jingyi Yu, and Hao Su. Tensorf: Tensorial radiance fields. In *European Conference on Computer Vision*, pages 333–350. Springer, 2022. 3
- [5] Yushuo Chen, Zerong Zheng, Zhe Li, Chao Xu, and Yebin Liu. Meshavatar: Learning high-quality triangular human avatars from multi-view videos. In *European Conference on Computer Vision*, 2024. 3
- [6] Zhaoxi Chen and Ziwei Liu. Relighting4d: Neural relightable human from videos. In *European Conference on Computer Vision*, pages 606–623. Springer, 2022. 3
- [7] Alvaro Collet, Ming Chuang, Pat Sweeney, Don Gillett, Dennis Evseev, David Calabrese, Hugues Hoppe, Adam Kirk, and Steve Sullivan. High-quality streamable free-viewpoint video. *ACM Transactions on Graphics (TOG)*, 34(4):69, 2015. 2, 3
- [8] R. L. Cook and K. E. Torrance. A reflectance model for computer graphics. *ACM Trans. Graph.*, 1(1):7–24, 1982. 5, 12
- [9] Paul Debevec. The light stages and their applications to photoreal digital actors. *SIGGRAPH Asia*, 2(4):1–6, 2012. 3
- [10] Paul Debevec, Tim Hawkins, Chris Tchou, Haarm-Pieter Duiker, Westley Sarokin, and Mark Sagar. Acquiring the reflectance field of a human face. In *Proceedings of the 27th annual conference on Computer graphics and interactive techniques*, pages 145–156, 2000.
- [11] Paul Debevec, Andreas Wenger, Chris Tchou, Andrew Gardner, Jamie Waese, and Tim Hawkins. A lighting reproduction approach to live-action compositing. *ACM Transactions on Graphics (TOG)*, 21(3):547–556, 2002. 3
- [12] Michael Deering, Stephanie Winner, Bic Schediwy, Chris Duffy, and Neil Hunt. The triangle processor and normal vector shader: a vlsi system for high performance graphics. In *Proceedings of the 15th Annual Conference on Computer Graphics and Interactive Techniques*, page 21–30, New York, NY, USA, 1988. Association for Computing Machinery. 6



- [13] Zheng Ding, Xuaner Zhang, Zhihao Xia, Lars Jebe, Zhuowen Tu, and Xiuming Zhang. Diffusionrig: Learning personalized priors for facial appearance editing. In *Proceedings of the IEEE/CVF Conference on Computer Vision and Pattern Recognition*, pages 12736–12746, 2023. 3
- [14] Mingsong Dou, Sameh Khamis, Yury Degtyarev, Philip Davidson, Sean Ryan Fanello, Adarsh Kowdle, Sergio Orts Escolano, Christoph Rhemann, David Kim, Jonathan Taylor, Pushmeet Kohli, Vladimir Tankovich, and Shahram Izadi. Fusion4d: real-time performance capture of challenging scenes. *ACM Trans. Graph.*, 35(4), 2016. 2
- [15] Yuanxing Duan, Fangyin Wei, Qiyu Dai, Yuhang He, Wenzheng Chen, and Baoquan Chen. 4d-rotor gaussian splatting: towards efficient novel view synthesis for dynamic scenes. In *ACM SIGGRAPH 2024 Conference Papers*, pages 1–11, 2024. 3
- [16] Sara Fridovich-Keil, Alex Yu, Matthew Tancik, Qinhong Chen, Benjamin Recht, and Angjoo Kanazawa. Plenoxels: Radiance fields without neural networks. In *Proceedings of the IEEE/CVF Conference on Computer Vision and Pattern Recognition*, pages 5501–5510, 2022. 3
- [17] Sara Fridovich-Keil, Giacomo Meanti, Frederik Rahbæk Warburg, Benjamin Recht, and Angjoo Kanazawa. K-planes: Explicit radiance fields in space, time, and appearance. In *Proceedings of the IEEE/CVF Conference on Computer Vision and Pattern Recognition*, pages 12479–12488, 2023. 3
- [18] Jian Gao, Chun Gu, Youtian Lin, Zhihao Li, Hao Zhu, Xun Cao, Li Zhang, and Yao Yao. Relightable 3d gaussians: Realistic point cloud relighting with brdf decomposition and ray tracing. In *European Conference on Computer Vision*, pages 73–89. Springer, 2025. 2, 3, 6, 7
- [19] Mathieu Garon, Pierre-Olivier Boulet, Jean-Philippe Doiron, Luc Beaulieu, and Jean-François Lalonde. Real-time high resolution 3d data on the hololens. In *2016 IEEE International Symposium on Mixed and Augmented Reality (ISMAR-Adjunct)*, pages 189–191. IEEE, 2016. 2
- [20] Chun Gu, Xiaofei Wei, Zixuan Zeng, Yuxuan Yao, and Li Zhang. Irgs: Inter-reflective gaussian splatting with 2d gaussian ray tracing. *arXiv preprint arXiv:2412.15867*, 2024. 3
- [21] Kaiwen Guo, Peter Lincoln, Philip Davidson, Jay Busch, Xueming Yu, Matt Whalen, Geoff Harvey, Sergio Orts-Escolano, Rohit Pandey, Jason Dourgarian, et al. The relightables: Volumetric performance capture of humans with realistic relighting. *ACM Transactions on Graphics (TOG)*, 38(6):1–19, 2019. 3
- [22] Marc Habermann, Lingjie Liu, Weipeng Xu, Gerard Pons-Moll, Michael Zollhoefer, and Christian Theobalt. Hdhumans: A hybrid approach for high-fidelity digital humans. *Proceedings of the ACM on Computer Graphics and Interactive Techniques*, 6(3):1–23, 2023. 3
- [23] Tim Hawkins, Jonathan Cohen, and Paul Debevec. A photometric approach to digitizing cultural artifacts. In *Proceedings of the 2001 conference on Virtual reality, archeology, and cultural heritage*, pages 333–342, 2001. 3
- [24] Yi-Hua Huang, Yang-Tian Sun, Ziyi Yang, Xiaoyang Lyu, Yan-Pei Cao, and Xiaojuan Qi. Sc-gs: Sparse-controlled gaussian splatting for editable dynamic scenes. In *Proceedings of the IEEE/CVF Conference on Computer Vision and Pattern Recognition*, pages 4220–4230, 2024. 3
- [25] Intel Corporation. Intel® open image denoise, 2025. 6
- [26] Mustafa Işık, Martin Rünz, Markos Georgopoulos, Taras Khakhulin, Jonathan Starck, Lourdes Agapito, and Matthias Nießner. Humanrf: High-fidelity neural radiance fields for humans in motion. *ACM Transactions on Graphics (TOG)*, 42(4):1–12, 2023. 3
- [27] Yuheng Jiang, Suyi Jiang, Guoxing Sun, Zhuo Su, Kaiwen Guo, Minye Wu, Jingyi Yu, and Lan Xu. Neuralhofusion: Neural volumetric rendering under human-object interactions. In *Proceedings of the IEEE/CVF Conference on Computer Vision and Pattern Recognition*, pages 6155–6165, 2022. 3
- [28] Yuheng Jiang, Kaixin Yao, Zhuo Su, Zhehao Shen, Haimin Luo, and Lan Xu. Instant-nvr: Instant neural volumetric rendering for human-object interactions from monocular rgbd stream. In *Proceedings of the IEEE/CVF Conference on Computer Vision and Pattern Recognition*, pages 595–605, 2023. 3
- [29] Yujiao Jiang, Qingmin Liao, Zhaolong Wang, Xiangru Lin, Zongqing Lu, Yuxi Zhao, Hanqing Wei, Jingrui Ye, Yu Zhang, and Zhijing Shao. Smplx-lite: A realistic and drivable avatar benchmark with rich geometry and texture annotations. In *2024 IEEE International Conference on Multimedia and Expo (ICME)*, pages 1–6, 2024. 3
- [30] Yuheng Jiang, Zhehao Shen, Yu Hong, Chengcheng Guo, Yize Wu, Yingliang Zhang, Jingyi Yu, and Lan Xu. Robust dual gaussian splatting for immersive human-centric volumetric videos. *ACM Transactions on Graphics (TOG)*, 43(6):1–15, 2024. 2, 3, 4, 12
- [31] Yuheng Jiang, Zhehao Shen, Penghao Wang, Zhuo Su, Yu Hong, Yingliang Zhang, Jingyi Yu, and Lan Xu. Hifi4g: High-fidelity human performance rendering via compact gaussian splatting. In *Proceedings of the IEEE/CVF Conference on Computer Vision and Pattern Recognition*, pages 19734–19745, 2024. 3
- [32] Yingwenqi Jiang, Jiadong Tu, Yuan Liu, Xifeng Gao, Xiaoxiao Long, Wenping Wang, and Yuexin Ma. Gaussian-shader: 3d gaussian splatting with shading functions for reflective surfaces. In *Proceedings of the IEEE/CVF Conference on Computer Vision and Pattern Recognition*, pages 5322–5332, 2024. 2, 3
- [33] James T Kajiya. The rendering equation. In *Proceedings of the 13th annual conference on Computer graphics and interactive techniques*, pages 143–150, 1986. 2, 5
- [34] Yoshihiro Kanamori and Yuki Endo. Relighting humans: occlusion-aware inverse rendering for full-body human images. *ACM Transactions on Graphics*, page 1–11, 2018. 3
- [35] Bernhard Kerbl, Georgios Kopanas, Thomas Leimkühler, and George Drettakis. 3d gaussian splatting for real-time radiance field rendering. *ACM Transactions on Graphics (ToG)*, 42(4):1–14, 2023. 2, 3, 6
- [36] Jason Lawrence, Ryan Overbeck, Todd Prives, Tommy Fortes, Nikki Roth, and Brett Newman. Project starline: A high-fidelity telepresence system. In *ACM SIGGRAPH 2024 Emerging Technologies*, pages 1–2, 2024. 2

- [37] Hao Li, Linjie Luo, Daniel Vlasic, Pieter Peers, Jovan Popović, Mark Pauly, and Szymon Rusinkiewicz. Temporally coherent completion of dynamic shapes. *ACM Trans. Graph.*, 31(1), 2012. 3
- [38] Zhan Li, Zhang Chen, Zhong Li, and Yi Xu. Spacetime gaussian feature splatting for real-time dynamic view synthesis. In *Proceedings of the IEEE/CVF Conference on Computer Vision and Pattern Recognition*, pages 8508–8520, 2024. 2, 3
- [39] Zhe Li, Zerong Zheng, Lizhen Wang, and Yebin Liu. Animatable gaussians: Learning pose-dependent gaussian maps for high-fidelity human avatar modeling. In *Proceedings of the IEEE/CVF Conference on Computer Vision and Pattern Recognition (CVPR)*, 2024. 3
- [40] Zhihao Liang, Qi Zhang, Ying Feng, Ying Shan, and Kui Jia. Gs-ir: 3d gaussian splatting for inverse rendering. In *Proceedings of the IEEE/CVF Conference on Computer Vision and Pattern Recognition*, pages 21644–21653, 2024. 2, 3, 6, 7
- [41] Matthew Loper, Naureen Mahmood, Javier Romero, Gerard Pons-Moll, and Michael J Black. Smpl: A skinned multi-person linear model. In *Seminal Graphics Papers: Pushing the Boundaries, Volume 2*, pages 851–866. 2023. 3
- [42] Jonathon Luiten, Georgios Kopanas, Bastian Leibe, and Deva Ramanan. Dynamic 3d gaussians: Tracking by persistent dynamic view synthesis. In *2024 International Conference on 3D Vision (3DV)*, pages 800–809. IEEE, 2024. 3
- [43] Diogo Luvizon, Vladislav Golyanik, Adam Kortylewski, Marc Habermann, and Christian Theobalt. Relightable neural actor with intrinsic decomposition and pose control, 2024. 3
- [44] Ben Mildenhall, Pratul P. Srinivasan, Matthew Tancik, Jonathan T. Barron, Ravi Ramamoorthi, and Ren Ng. Nerf: Representing scenes as neural radiance fields for view synthesis. In *Computer Vision – ECCV 2020*, pages 405–421, Cham, 2020. Springer International Publishing. 3
- [45] Nicolas Moenne-Loccoz, Ashkan Mirzaei, Or Perel, Riccardo de Lutio, Janick Martinez Esturo, Gavriel State, Sanja Fidler, Nicholas Sharp, and Zan Gojcic. 3d gaussian ray tracing: Fast tracing of particle scenes. *ACM Transactions on Graphics and SIGGRAPH Asia*, 2024. 2, 5
- [46] Thomas Müller, Alex Evans, Christoph Schied, and Alexander Keller. Instant neural graphics primitives with a multiresolution hash encoding. *ACM Trans. Graph.*, 41(4):102:1–102:15, 2022. 3
- [47] New House Internet Services B.V. PTGui Stitching Software, 2025. 2, 5
- [48] Haokai Pang, Heming Zhu, Adam Kortylewski, Christian Theobalt, and Marc Habermann. Ash: Animatable gaussian splats for efficient and photoreal human rendering. In *Proceedings of the IEEE/CVF Conference on Computer Vision and Pattern Recognition*, pages 1165–1175, 2024. 3
- [49] Sida Peng, Yuanqing Zhang, Yinghao Xu, Qianqian Wang, Qing Shuai, Hujun Bao, and Xiaowei Zhou. Neural body: Implicit neural representations with structured latent codes for novel view synthesis of dynamic humans. In *Proceedings of the IEEE/CVF Conference on Computer Vision and Pattern Recognition*, pages 9054–9063, 2021. 3
- [50] Albert Pumarola, Enric Corona, Gerard Pons-Moll, and Francesc Moreno-Noguer. D-nerf: Neural radiance fields for dynamic scenes. In *Proceedings of the IEEE/CVF Conference on Computer Vision and Pattern Recognition*, pages 10318–10327, 2021. 3
- [51] RenderPeople. Renderpeople, 2025. 7
- [52] Christopher M. Schlick. An inexpensive brdf model for physically-based rendering. *Computer Graphics Forum*, 13, 1994. 12
- [53] Ruizhi Shao, Zerong Zheng, Hanzhang Tu, Boning Liu, Hongwen Zhang, and Yebin Liu. Tensor4d: Efficient neural 4d decomposition for high-fidelity dynamic reconstruction and rendering. In *Proceedings of the IEEE/CVF Conference on Computer Vision and Pattern Recognition*, pages 16632–16642, 2023. 3
- [54] Yahao Shi, Yanmin Wu, Chenming Wu, Xing Liu, Chen Zhao, Haocheng Feng, Jingtuo Liu, Liangjun Zhang, Jian Zhang, Bin Zhou, et al. Gir: 3d gaussian inverse rendering for relightable scene factorization. *arXiv preprint arXiv:2312.05133*, 2023. 2
- [55] Liangchen Song, Anpei Chen, Zhong Li, Zhang Chen, Lele Chen, Junsong Yuan, Yi Xu, and Andreas Geiger. Nerf-player: A streamable dynamic scene representation with decomposed neural radiance fields. *IEEE Transactions on Visualization and Computer Graphics*, 29(5):2732–2742, 2023. 3
- [56] Pratul P Srinivasan, Boyang Deng, Xiuming Zhang, Matthew Tancik, Ben Mildenhall, and Jonathan T Barron. Nerv: Neural reflectance and visibility fields for relighting and view synthesis. In *Proceedings of the IEEE/CVF Conference on Computer Vision and Pattern Recognition*, pages 7495–7504, 2021. 2
- [57] Guoxing Sun, Xin Chen, Yizhang Chen, Anqi Pang, Pei Lin, Yuheng Jiang, Lan Xu, Jingyi Yu, and Jingya Wang. Neural free-viewpoint performance rendering under complex human-object interactions. In *Proceedings of the 29th ACM International Conference on Multimedia*, pages 4651–4660, 2021. 3
- [58] Guoxing Sun, Rishabh Dabral, Heming Zhu, Pascal Fua, Christian Theobalt, and Marc Habermann. Real-time free-view human rendering from sparse-view rgb videos using double unprojected textures. *arXiv preprint arXiv:2412.13183*, 2024. 3
- [59] Jiakai Sun, Han Jiao, Guangyuan Li, Zhanjie Zhang, Lei Zhao, and Wei Xing. 3dstream: On-the-fly training of 3d gaussians for efficient streaming of photo-realistic free-viewpoint videos. In *Proceedings of the IEEE/CVF Conference on Computer Vision and Pattern Recognition*, pages 20675–20685, 2024. 3
- [60] Xin Suo, Yuheng Jiang, Pei Lin, Yingliang Zhang, Minye Wu, Kaiwen Guo, and Lan Xu. Neuralhumanfvv: Real-time neural volumetric human performance rendering using rgb cameras. In *Proceedings of the IEEE/CVF Conference on Computer Vision and Pattern Recognition*, pages 6226–6237, 2021. 3
- [61] D. Tajima, Y. Kanamori, and Y. Endo. Relighting humans in the wild: Monocular full-body human relighting with do-

- main adaptation. *Computer Graphics Forum*, page 205–216, 2021. 3
- [62] Edgar Tretschk, Ayush Tewari, Vladislav Golyanik, Michael Zollhöfer, Christoph Lassner, and Christian Theobalt. Non-rigid neural radiance fields: Reconstruction and novel view synthesis of a dynamic scene from monocular video. In *Proceedings of the IEEE/CVF International Conference on Computer Vision*, pages 12959–12970, 2021. 3
- [63] Delio Vicini, Sébastien Speierer, and Wenzel Jakob. Path replay backpropagation: differentiating light paths using constant memory and linear time. *ACM Trans. Graph.*, 40(4):108:1–108:14, 2021. 7
- [64] Liao Wang, Qiang Hu, Qihan He, Ziyu Wang, Jingyi Yu, Tinne Tuytelaars, Lan Xu, and Minye Wu. Neural residual radiance fields for streamably free-viewpoint videos. In *Proceedings of the IEEE/CVF Conference on Computer Vision and Pattern Recognition*, pages 76–87, 2023. 3
- [65] Penghao Wang, Zhirui Zhang, Liao Wang, Kaixin Yao, Siyuan Xie, Jingyi Yu, Minye Wu, and Lan Xu. V<sup>3</sup>: Viewing volumetric videos on mobiles via streamable 2d dynamic gaussians. *ACM Transactions on Graphics (TOG)*, 43(6):1–13, 2024. 2
- [66] Chung-Yi Weng, Brian Curless, Pratul P Srinivasan, Jonathan T Barron, and Ira Kemelmacher-Shlizerman. Humannerf: Free-viewpoint rendering of moving people from monocular video. In *Proceedings of the IEEE/CVF conference on computer vision and pattern Recognition*, pages 16210–16220, 2022. 3
- [67] Andreas Wenger, Andrew Gardner, Chris Tchou, Jonas Unger, Tim Hawkins, and Paul Debevec. Performance relighting and reflectance transformation with time-multiplexed illumination. *ACM Transactions on Graphics (TOG)*, 24(3):756–764, 2005. 3
- [68] Tim Weyrich, Wojciech Matusik, Hanspeter Pfister, Bernd Bickel, Craig Donner, Chien Tu, Janet McAndless, Jinho Lee, Addy Ngan, Henrik Wann Jensen, et al. Analysis of human faces using a measurement-based skin reflectance model. *ACM Transactions on Graphics (ToG)*, 25(3):1013–1024, 2006. 3
- [69] Guanjun Wu, Taoran Yi, Jiemin Fang, Lingxi Xie, Xiaopeng Zhang, Wei Wei, Wenyu Liu, Qi Tian, and Xinggang Wang. 4d gaussian splatting for real-time dynamic scene rendering. In *Proceedings of the IEEE/CVF Conference on Computer Vision and Pattern Recognition*, pages 20310–20320, 2024. 3
- [70] Wenqi Xian, Jia-Bin Huang, Johannes Kopf, and Changil Kim. Space-time neural irradiance fields for free-viewpoint video. In *Proceedings of the IEEE/CVF Conference on Computer Vision and Pattern Recognition*, pages 9421–9431, 2021. 3
- [71] Zhen Xu, Sida Peng, Chen Geng, Linzhan Mou, Zihan Yan, Jiaming Sun, Hujun Bao, and Xiaowei Zhou. Relightable and animatable neural avatar from sparse-view video. In *Proceedings of the IEEE/CVF Conference on Computer Vision and Pattern Recognition*, pages 990–1000, 2024. 3
- [72] Zhen Xu, Yinghao Xu, Zhiyuan Yu, Sida Peng, Jiaming Sun, Hujun Bao, and Xiaowei Zhou. Representing long volumetric video with temporal gaussian hierarchy. *ACM Transactions on Graphics (TOG)*, 43(6):1–18, 2024. 3
- [73] Zeyu Yang, Zijie Pan, Xiatian Zhu, Li Zhang, Yu-Gang Jiang, and Philip H. S. Torr. 4d gaussian splatting: Modeling dynamic scenes with native 4d primitives. 2024. 3
- [74] Yao Yao, Jingyang Zhang, Jingbo Liu, Yihang Qu, Tian Fang, David McKinnon, Yanghai Tsin, and Long Quan. Neif: Neural incident light field for physically-based material estimation. In *European Conference on Computer Vision*, pages 700–716. Springer, 2022. 2
- [75] Tao Yu, Zerong Zheng, Kaiwen Guo, Pengpeng Liu, Qionghai Dai, and Yebin Liu. Function4d: Real-time human volumetric capture from very sparse consumer rgbd sensors. In *Proceedings of the IEEE/CVF Conference on Computer Vision and Pattern Recognition*, pages 5746–5756, 2021. 3
- [76] Chong Zeng, Guojun Chen, Yue Dong, Pieter Peers, Hongzhi Wu, and Xin Tong. Relighting neural radiance fields with shadow and highlight hints. In *ACM SIGGRAPH 2023 Conference Proceedings*, pages 1–11, 2023. 3
- [77] Chong Zeng, Yue Dong, Pieter Peers, Youkang Kong, Hongzhi Wu, and Xin Tong. Dilightnet: Fine-grained lighting control for diffusion-based image generation. In *Special Interest Group on Computer Graphics and Interactive Techniques Conference Conference Papers '24*, page 1–12. ACM, 2024. 3
- [78] Baowen Zhang, Chuan Fang, Rakesh Shrestha, Yixun Liang, Xiaoxiao Long, and Ping Tan. Rade-gs: Rasterizing depth in gaussian splatting. *arXiv preprint arXiv:2406.01467*, 2024. 2, 4
- [79] Longwen Zhang, Ziyu Wang, Qixuan Zhang, Qiwei Qiu, Anqi Pang, Haoran Jiang, Wei Yang, Lan Xu, and Jingyi Yu. Clay: A controllable large-scale generative model for creating high-quality 3d assets. *ACM Transactions on Graphics (TOG)*, 43(4):1–20, 2024. 2, 4
- [80] Shuai Zhang, Guanjun Wu, Xinggang Wang, Bin Feng, and Wenyu Liu. Dynamic 2d gaussians: Geometrically accurate radiance fields for dynamic objects. *arXiv preprint arXiv:2409.14072*, 2024. 6, 7
- [81] Xiuming Zhang, Pratul P Srinivasan, Boyang Deng, Paul Debevec, William T Freeman, and Jonathan T Barron. Nerfactor: Neural factorization of shape and reflectance under an unknown illumination. *ACM Transactions on Graphics (ToG)*, 40(6):1–18, 2021. 2, 3
- [82] Fuqiang Zhao, Yuheng Jiang, Kaixin Yao, Jiakai Zhang, Liao Wang, Haizhao Dai, Yuhui Zhong, Yingliang Zhang, Minye Wu, Lan Xu, and Jingyi Yu. Human performance modeling and rendering via neural animated mesh. *ACM Trans. Graph.*, 41(6), 2022. 3
- [83] Yang Zheng, Qingqing Zhao, Guandao Yang, Wang Yifan, Donglai Xiang, Florian Dubost, Dmitry Lagun, Thabo Beeler, Federico Tombari, Leonidas Guibas, et al. Physavatar: Learning the physics of dressed 3d avatars from visual observations. In *European Conference on Computer Vision*, pages 262–284. Springer, 2025. 3
- [84] Zerong Zheng, Xiaochen Zhao, Hongwen Zhang, Boning Liu, and Yebin Liu. Avatarrex: Real-time expressive full-body avatars. *ACM Transactions on Graphics (TOG)*, 42(4):1–19, 2023. 3



[85] Heming Zhu, Fangneng Zhan, Christian Theobalt, and Marc Habermann. Trihuman: a real-time and controllable tri-plane representation for detailed human geometry and appearance synthesis. *ACM Transactions on Graphics*, 44(1): 1–17, 2024. 3

## A. Energy Term

To model human motion using Gaussian sequences, we first employ the color energy  $E_{\text{color}}$  during the training process:

$$E_{\text{color}} = (1 - \lambda_{\text{color}})\mathcal{L}_1 + \lambda_{\text{color}}\mathcal{L}_{\text{D-SSIM}}, \quad (8)$$

where  $\mathcal{L}_1$  is the  $L_1$  photometric loss and  $\mathcal{L}_{\text{D-SSIM}}$  is the D-SSIM term. We then employ a smooth regularizer to constrain the joint Gaussians motion locally as-rigid-as-possible (ARAP):

$$E_{\text{smooth}} = \sum_i \sum_{k \in \mathcal{N}(i)} w_{i,k} \left\| R \left( q_{i,t}^j * q_{i,t-1}^{j-1} \right) \left( p_{k,t-1}^j - p_{i,t-1}^j \right) - \left( p_{k,t}^j - p_{i,t}^j \right) \right\|_2^2, \quad (9)$$

where  $\mathcal{N}(i)$  represents the set of neighboring joint Gaussian kernels of  $i$ ,  $R(\cdot)$  converts quaternion back into a rotation matrix and  $w_{i,k}$  corresponds to the blending weights according to DualGS [30]. Furthermore, we apply the temporal regularizer  $E_{\text{temp}}$  to promote coherent appearances by constraining Gaussian attributes  $(C_{i,t}^j, \sigma_{i,t}^j, s_{i,t}^j)$  to be consistent with the previous frame:

$$E_{\text{temp}} = \sum_{a \in \{C, \sigma, s\}} \lambda_a \|a_{i,t} - a_{i,t-1}\|_2^2, \quad (10)$$

Together with  $E_{\text{normal}}$  we mentioned above, the overall energy term in our 4D Gaussian modeling is expressed as:

$$E = \lambda_{\text{color}}E_{\text{color}} + \lambda_{\text{smooth}}E_{\text{smooth}} + \lambda_{\text{temp}}E_{\text{temp}} + \lambda_{\text{normal}}E_{\text{normal}}, \quad (11)$$

which helps us obtain accurate geometric information while modeling human performance sequences.

## B. Base Color Decomposition

To compute base color, we ignore the effect of indirect illumination caused by reflections on the surface of the human body, the rendering equation can be approximated as:

$$L_o(x, \omega_o) \approx \int_{\Omega} f_r(x, \omega_i, \omega_o) V^{\text{env}}(x, \omega_i) L_i^{\text{env}}(\omega_i) (\mathbf{n} \cdot \omega_i) d\omega_i, \quad (12)$$

where  $x$  and  $\mathbf{n}$  are the surface point and its normal vector,  $f_r$  is the Bidirectional Reflectance Distribution Function (BRDF),  $L_o(x, \omega_o)$  denotes the outgoing radiance in direction  $\omega_o$ .

We decompose the BRDF term  $f_r$  into two components, the diffuse term  $f_{r_d}$  and the specular term  $f_{r_s}$ , where we

use the Lambertian model for  $f_{r_d}$  and Cook-Torrance microfacet specular shading model [8] for  $f_{r_s}$ :

$$f_r(x, \omega_i, \omega_o) = f_{r_d}(x, \omega_i, \omega_o) + f_{r_s}(x, \omega_i, \omega_o), \quad (13)$$

$$f_{r_d}(x, \omega_i, \omega_o) = \frac{1 - F}{\pi} \rho(x), \quad (14)$$

$$f_{r_s}(x, \omega_i, \omega_o) = \frac{DGF}{4(\mathbf{n} \cdot \omega_i)(\mathbf{n} \cdot \omega_o)}, \quad (15)$$

where  $D$ ,  $G$ ,  $F$  are respectively the GGX normal distribution function (NDF), the geometric attenuation function, and the approximated Fresnel term. We then split  $L_o$  into two parts:

$$L_o(x, \omega_o) = \int_{\Omega} (f_{r_d} + f_{r_s}) \mathcal{L} d\omega_i, \quad (16)$$

$$= \int_{\Omega} f_{r_d} \mathcal{L} d\omega_i + \int_{\Omega} f_{r_s} \mathcal{L} d\omega_i, \quad (17)$$

$$= \frac{\rho(x)}{\pi} \int_{\Omega} (1 - F) \mathcal{L} d\omega_i + \int_{\Omega} f_{r_s} \mathcal{L} d\omega_i, \quad (18)$$

where  $\mathcal{L} = V^{\text{env}}(x, \omega_i) L_i^{\text{env}}(\omega_i) (\mathbf{n} \cdot \omega_i)$ .

The  $D$  and  $G$  in  $f_{r_s}$  are both irrelevant with the base color  $\rho$ . For the Fresnel term  $F$ , we use the Schlick Fresnel approximation [52]:

$$F = F_0 + (1 - F_0) (1 - (\mathbf{h} \cdot \omega_o))^5, \quad (19)$$

where  $\mathbf{h} = \frac{\omega_o + \omega_i}{\|\omega_o + \omega_i\|}$ ,  $F_0$  represents the specular reflectance at normal incidence and is achromatic for dielectrics and chromatic for metals. Since the human body is mostly composed of dielectric materials, we assume  $F_0 = 0.04$ , so that  $F$  is also irrelevant with  $\rho$ . Consequently, we can solve the base color  $\rho$  from Eq. 18:

$$\rho(x) = \frac{\pi (L_o(x, \omega_o) - \int_{\Omega} f_{r_s} \mathcal{L} d\omega_i)}{\int_{\Omega} (1 - F) \mathcal{L} d\omega_i}. \quad (20)$$

## C. Additional Evaluations

In this section, we present more details on the qualitative comparison conducted on synthetic human data, including normal, roughness, base color, AO, and relight rendering effects in Fig. 9.

## D. Applications

In Fig. 10, we showcase the application of watching an actor dancing in a scene with varying lighting. Viewers can immerse themselves in a realistic environment with dramatic lighting changes, observing the actor's dance performance seamlessly integrated into the surroundings. We can capture, process, and generate high-fidelity human 4D assets with our dome cameras and BEAM pipeline, reproducing outstanding performances in different scenes and lightings.

At the same time, our compatibility with the traditional CG pipeline allows us to edit scenes in the Unity plugin we developed or integrate multiple human performances, as shown in Fig. 11. We can align multiple performances through CG platform, edit the scene and lighting, and present stunning visual effects of the performances.

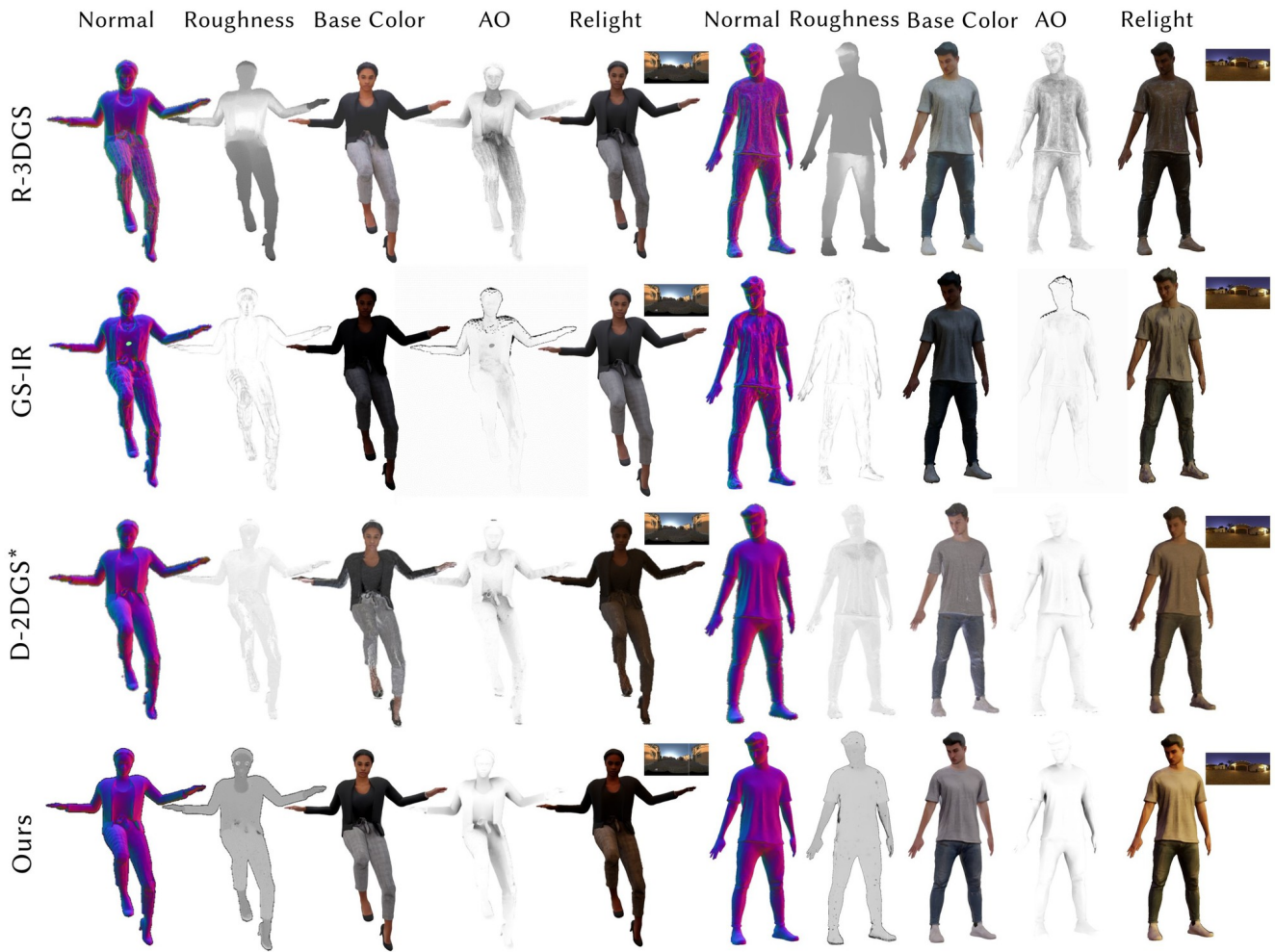


Figure 9. We present additional comparison results on synthetic humans, demonstrating the high-quality relighting capabilities of our method.



Figure 10. We demonstrate our VR application on PICO, enabling an immersive experience with relightable volumetric video.





Figure 11. We showcase our custom Unity plugin for relightable 4D Gaussian assets. Our relightable 4D Gaussians are CG-friendly, supporting scene and lighting environment editing within Unity.